Research Article

Local dose-dense chemotherapy for triple-negative breast cancer via minimally invasive implantation of 3D printed devices

*Noehyun Myung, Hyun-Wook Kang**

Department of Biomedical Engineering, Ulsan National Institute of Science and Technology (UNIST), Ulju-gun 44919, South Korea

ARTICLE INFO

ABSTRACT

Dose-dense chemotherapy is the preferred first-line therapy for triple-negative breast cancer (TNBC), a highly aggressive disease with a poor prognosis. This treatment uses the same drug doses as conventional chemotherapy but with shorter dosing intervals, allowing for promising clinical outcomes with intensive treatment. However, the frequent systemic administration used for this treatment results in systemic toxicity and low patient compliance, limiting therapeutic efficacy and clinical benefit. Here, we report local dose-dense chemotherapy to treat TNBC by implanting 3D printed devices with time-programmed pulsatile release profiles. The implantable device can control the time between drug releases based on its internal microstructure design, which can be used to control dose density. The device is made of biodegradable materials for clinical convenience and designed for minimally invasive implantation via a trocar. Dose density variation of local chemotherapy using programmable release enhances anti-cancer effects *in vitro* and *in vivo*. Under the same dose density conditions, device-based chemotherapy shows a higher anti-cancer effect and less toxic response than intratumoral injection. We demonstrate local chemotherapy utilizing the implantable device that simulates the drug dose, number of releases, and treatment duration of the dose-dense AC (doxorubicin and cyclophosphamide) regimen preferred for TNBC treatment. Dose density modulation inhibits tumor growth, metastasis, and the expression of drug resistance-related proteins, including p-glycoprotein and breast cancer resistance protein. To the best of our knowledge, local dose-dense chemotherapy has not been reported, and our strategy can be expected to be utilized as a novel alternative to conventional therapies and improve anti-cancer efficiency.

---

* Corresponding author.
  E-mail address: hkang@unist.ac.kr (H.-W. Kang).
  Peer review under responsibility of Shenyang Pharmaceutical University.

1. Introduction

Breast cancer is the most common tumor worldwide and the second leading cause of cancer-related death in women, following lung cancer [1]. It is categorized into subtypes based on the presence of estrogen receptors (ER), progesterone receptors (PR), and human epidermal growth factor receptor 2 (HER2). Triple-negative breast cancer (TNBC) is a subtype lacking these receptors and represents 15%−20% of all breast cancer cases [2]. TNBC is aggressive, with a significant risk of metastasis and recurrence, and has one of the worst prognoses of all breast cancers [3]. Due to limited therapeutic targets and its heterogeneity, targeted therapy is challenging, and chemotherapy remains the primary treatment option [4]. Pharmaceutical companies have explored new drugs to enhance chemotherapy effectiveness, but they face significant drawbacks, including prohibitive costs, lengthy development time, and low success rates [5,6]. As an alternative approach, researchers are exploring ways to enhance TNBC chemotherapy by optimizing the combination [7,8], order [9–11], and dose of existing anti-cancer drugs [12].

Dose-dense chemotherapy is a preferred first-line treatment for TNBC that delivers the same drugs as standard chemotherapy but with shorter intervals between cycles [13]. Based on the Gompertz growth model and Norton-Simon hypothesis, this strategy takes advantage of the increased effectiveness of chemotherapy in the early stages of a tumor with a rapid growth rate [14,15]. Dose-dense chemotherapy effectively kills cancer cells by administering drugs intensively during this period [16]. Especially, it uses a combination of doxorubicin (DOX, Adriamycin®) and cyclophosphamide (CYP), known as dose-dense AC regimens, which is representative of TNBC treatment [17]. This regimen has been used alone or with the sequential administration of paclitaxel [18]. However, like other chemotherapies, dose-dense chemotherapy that administers anti-cancer drugs via systemic routes, such as intravenous injection, has limited amounts of drug delivered to the tumor, systemic toxicity, and low patient compliance due to frequent administration.

Local drug delivery for dose-dense chemotherapy is a promising solution to overcome the limitations of systemic drug administration and enhance therapeutic efficacy. For local chemotherapy, a local drug delivery system (LDDS) can be implanted or injected into or around a tumor to deliver drugs directly to the tumor instead of the usual dosing strategies that cause systemic toxicity [19–21]. A prime example is the Gliadel® wafer (camustine implant) used for the local treatment of malignant gliomas [22]. Various LDDSs for TNBC chemotherapy have been introduced, including injectable hydrogels [23,24], micro/nanoparticles [25,26], and implantable scaffolds manufactured via mold casting [27,28], electrospinning [29,30], or 3D printing [31,32]. These systems can deliver high concentrations of drugs directly to tumors without loss and have demonstrated superior anti-cancer effects compared to conventional systemic administration. However, most LDDSs have a simple sustained release profile, which limits their pharmacokinetic characterization for dose-dense chemotherapy applications. The dose density in this chemotherapy refers to the intervals between cycles [33]. The dose density is increased for higher dose intensity by reducing the time between releases while keeping the total number of drug releases the same [13]. Pulsatile drug release with adjustable time intervals between releases can be utilized to control dose density. Strategies involving mechanical actuation (manual or battery-operated) and materials that respond to stimuli, such as lasers, ultrasound, and magnetic fields, have been considered [34–39]. However, they have critical challenges to their direct clinical application, including FDA approval hurdles of chemically synthesized materials, low patient compliance due to the need for repeated stimulation or manipulation, and the use of non-biodegradable materials and batteries requiring surgical removal. Therefore, local dose-dense chemotherapy requires implantable systems made of biodegradable materials to adjust dose density without additional manipulation for pulsatile drug release.

Our previous work used 3D printing to develop implantable devices with a programmable release profile for personalized medicine [40]. This device was constructed using FDA-approved and commercially available biodegradable materials for human use [41]. The design modulation of the device's printing layer allowed precise control over various parameters such as drug dose, combination, release rate, release duration, and release initiation time. For instance, the number of drug releases could be adjusted by altering the number of drug layers, and the time between releases could be extended by increasing the porous layer thickness between the drug layers. Moreover, the previous studies demonstrated that the devices evaluated similar pharmacokinetics in both *in vitro* and *in vivo* environments, making them suitable for implementing dose-dense chemotherapy through local delivery while effectively controlling dose density.

In this study, a novel local chemotherapy strategy implementing dose-dense AC regimens with the 3D printed device was demonstrated to treat TNBC. This therapy uses the time-programmed pulsatile release properties of the implanted device to destroy tumor cells and deliver the drug directly to the tumor at a therapeutically appropriate density by adjusting the interval of drug releases. The device could be fabricated through 3D co-printing of poly-ε-caprolactone (PCL) and Pluronic F127 (PF127) gel with DOX and CYP, which can be minimally invasively implanted to contact TNBC tumors via trocar injection (Fig. 1A). First, *in vitro* and *in vivo* experiments were performed in which devices with various drug release intervals were applied to the TNBC cell line and syngeneic TNBC models, respectively, to verify the enhancement of the anti-cancer effect of the local dose-dense chemotherapy according to the change in dose density. Furthermore, compared to local chemotherapy using intratumoral (IT) injection, we found that local dose-dense chemotherapy using the 3D printed devices had superior therapeutic efficacy in destroying tumors and lower side effects. The device that considers the dose, number of doses, and overall treatment duration of the dose-dense AC regimen used in clinical practice was performed in a syngeneic TNBC mouse model. Tumor growth inhibition and metastasis suppression were observed by diversifying the dose density, a key parameter of this therapy, to enhance the anti-cancer effect (Fig. 1B). Interestingly, we validated an association
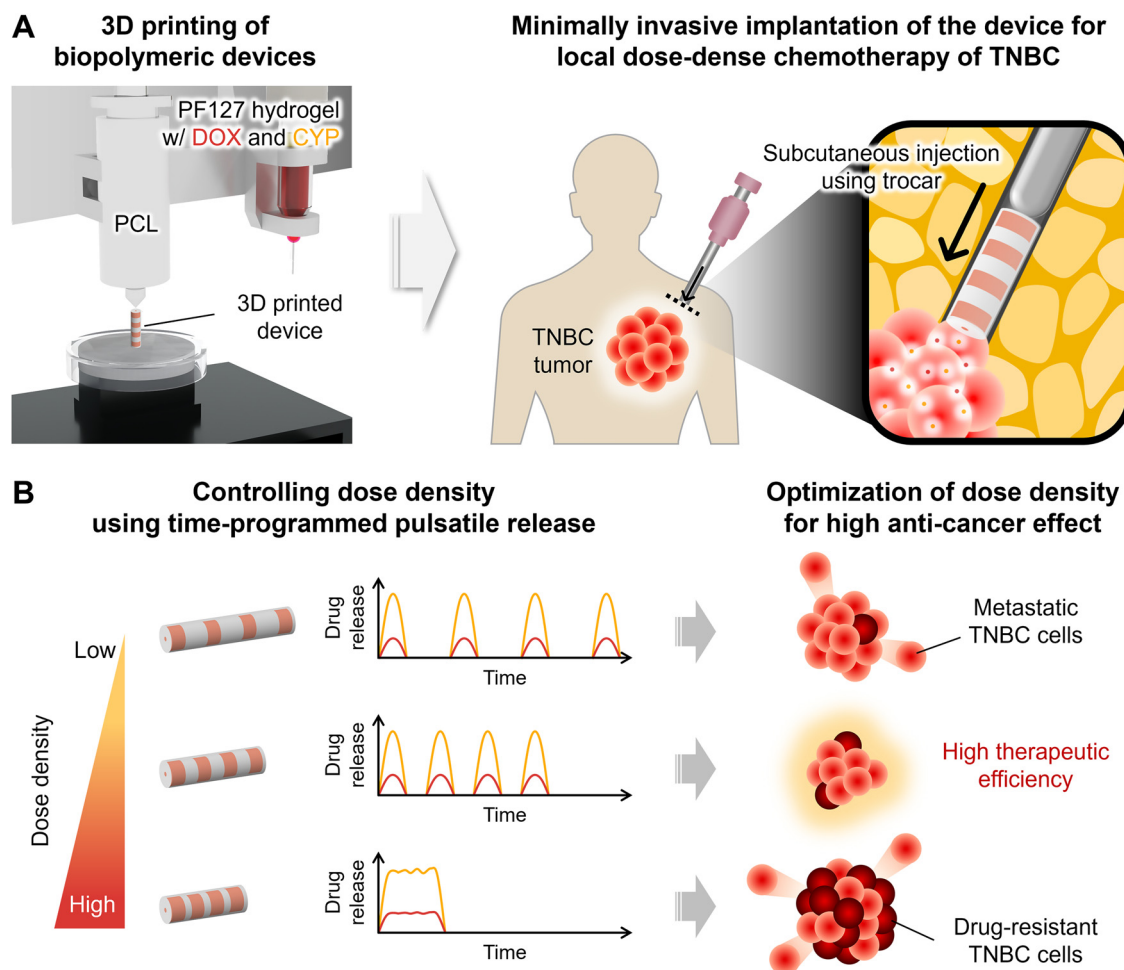
Fig. 1 – Schematics of local dose-dense chemotherapy using 3D printed devices with time-programmed pulsatile release profile for TNBC. (A) Preparation of a 3D printed device with DOX and CYP and its implantation to TNBC tumors. (B) Optimization of dose density for local dose-dense AC chemotherapy using 3D printed devices to improve therapeutic efficiency.

between increasing the dose density of this regimen and the expression of drug resistance-associated proteins, suggesting the need for appropriate dose density in therapy to improve therapeutic efficiency. To the best of our knowledge, the application of dose-dense chemotherapy using local delivery to the treatment of TNBC has not been reported, and our strategy can be expected to be widely utilized not only in TNBC but also in other diseases to increase the efficiency of existed treatment using systemic administration approach.

2.　　Materials and methods

2.1.　Material

PCL was from Polysciences, Inc. (Warrington, PA, USA) and PF127 was from Sigma-Aldrich (St. Louis, MO, USA); DOX was from MedChemExpress (Monmouth Junction, NJ, USA) and CYP was from Sigma-Aldrich; The alamarBlue solution was obtained from Invitrogen (AlamarBlue^{TM} Cell Viability

Reagent; Carlsbad, CA, USA); D-luciferin was from GoldBio, St. Louis, (MO, USA).

2.2.　Cell culture

A luciferase-expressing 4T1 (4T1-Luc2) (CRL-2539-LUC2), a triple-negative mouse breast cancer cell line, was obtained from the American Type Culture Collection (ATCC, Manassas, VA, USA). RPMI 1640 medium (LM 011–03; Welgene, Daegu, South Korea); 10% fetal bovine serum (FBS-22A; Capricorn Scientific) and 1% penicillin/streptomycin (PS-B; Capricorn Scientific). Cells were incubated in a humidified environment of 5% CO_2 at 37 °C.

2.3.　Preparation and characterization of 3D printed devices

3D printed devices were fabricated using PCL and PF127 gel with drugs as previously described [40]. Briefly, the biopolymer-based devices were made by a pneumatic

extrusion-based 3D printing technique. PCL granules were melted inside a metal syringe with a 200 µm cone-shaped metal nozzle at 90 °C. DOX and CYP were mixed with the 30% (w/v) PF127 solution to prepare a drug-loaded gel ink. The drug concentrations used varied according to experiments (Table S1). The gel ink was loaded into a plastic syringe with a 250 µm needle nozzle. A plunger was placed on the gel ink to push the gel out under air pressure. We prepared and maintained a humid environment at 21 °C suitable for printing. The PCL was printed at 250 kPa with an 80–140 mm/min feed rate. The drug-loaded ink was also pneumatically extruded at 100 kPa with a 60–120 mm/min feed rate. The devices were fabricated as designed in the visualized motion program, and the designs were adjusted according to the experiments.

Rheological tests on PF127 gel were performed utilizing a rheometer (HAAKE MARS III; Thermo Scientific, MA, USA). The viscosity of PF127 gel is measured by shear sweep analysis at 0.1–100 s^{-1} using a 20 mm parallel plate at 21 °C (printing temperature) and 37 °C (body temperature). The storage modulus (G') and loss modulus (G'') of PF127 gel were also measured by oscillation frequency sweep tests (frequency: 0.1–100 Hz, temperature: 21 °C and 37 °C).

The surface morphologies of the device layers were characterized by field emission scanning electron microscopy (FE-SEM) (SU8220; Hitachi High-Technologies Corp., Tokyo, Japan). Pt-coated samples were imaged by operating the FE-SEM at 10 kV. SEM images were quantified using ImageJ software (version 1.54d; National Institutes of Health, Bethesda, MD, USA).

2.4. In vitro drug release study

The devices were sunk in 3 ml phosphate-buffered saline (PBS, pH 7.4) and incubated at 37 °C [42]. A 200 µl aliquot of the solution was collected every 6 h and replaced with an equal amount of fresh PBS. The amount of released DOX and CYP was measured using a UV–vis spectrophotometer (SpectraMax Plus 384; Molecular Devices, Sunnyvale, CA, USA) at 479 nm and 210 nm, respectively, against standard curves with the known concentration of DOX and CYP [40,43].

2.5. In vitro anti-cancer activity

The in vitro anti-cancer activity of the DOX-loaded device (DOX device) with varying dose density was evaluated. 4T1-Luc2 cells were seeded at a density of 1,000 cells/well in 24-well plates and cultured for 24 h. The capsular devices were prepared with various dose densities and DOX-loaded PF127 gel ink at a 0–0.1% (w/v) concentration. To prevent the device from restricting the cells' growth space, PCL mesh structures were placed in the well plate, and devices were placed on top of this structure. The culture medium was changed daily, and the device was removed after 9 d of incubation. After 24 h recovery period, cell viability and proliferation activity were evaluated. Viability was assessed by fluorescence imaging of live cells using the Live/Dead Viability/Cytotoxicity kit (L3224; Thermo Scientific, Waltham, MA, USA). After washing with PBS, the samples were stained with calcein-AM (0.5 µl/ml) and ethidium homodimer (2 µl/ml) for 30 min at room temperature. The stained cells were observed by fluorescent

microscopy. The numbers of live cells were quantified by QuPath software (version 0.4.3). The proliferation activity of 4T1-Luc2 cells was measured by an alamarBlue assay. The alamarBlue solution was mixed with culture media to prepare a 10% alamarBlue solution. After washing with PBS, 200 µl of 10% alamarBlue solution was added to samples and incubated for 2 h. A 100 µl aliquot of the reacted medium was collected and measured the fluorescence intensity at an excitation wavelength of 544 nm and an emission wavelength of 590 nm using a Multi-Mode Microplate Reader (Synergy™ Neo2; BioTek Instruments, Inc., Winooski, VT, USA).

2.6. Syngeneic TNBC mouse models and treatments

Female BALB/c mice (6 weeks old) were purchased from Orient Bio (Seongnam, South Korea). 4T1-Luc2 cells were adjusted to 1×10^5 cells/ml cell density in a PBS solution. 100 µl of cell suspensions were inoculated into mice's inguinal right mammary fat pad under 1.5%–2% isoflurane gas anesthesia. A digital vernier caliper measured tumor sizes, and the volume was calculated according to the following equation.

$$\text{Tumor volume}\left(\text{mm}^3\right) = (4/3)\pi \times (W/2)^2 \times (L/2)$$

Where, W and L are the width and length of the tumor, respectively. All treatments were performed when tumor volumes reached 75 mm^3.

To evaluate the in vivo anti-cancer effect of the DOX device according to adjusted dose density, DOX devices (5 mg/kg body weight; release five times) with various dose densities (120 h, 72 h, 24 h, and 0 h) were prepared. 4T1-Luc2 tumor-bearing mice were randomly divided into seven groups ($n = 6$): untreated, drug-free device, IT injection (5 mg/kg DOX, 5 times, 72 h), device-120 h, device-72 h, device-24 h, and device-0 h. The device was implanted minimally invasively using a trocar into BALB/c mice under anesthesia. The implanted device was positioned so the outlet layer was in contact with the tumor. For the IT group, 100 µl DOX solution was IT injected into mice every 4 d for five injections. During the treatment period, the tumor volume and the body weights were measured every 3–4 d, respectively, for 28 d. The survival rate of all mice was also monitored for 28 d.

AC solutions containing DOX (5 mg/kg) and CYP (20 mg/kg) were prepared to validate the efficacy of localized dose-dense AC chemotherapy using the IT injection. 4T1-Luc2 tumor-bearing mice were randomly divided into six groups ($n = 6$): PBS (168 h), DOX (5 mg/kg, 168 h), CYP (20 mg/kg, 168 h), AC-168 h, AC-72 h, and AC-240 h. Solutions were IT injected four times at set time intervals per group. The tumor volume and the body weights were measured every 7 d for 42 d during the treatment period, respectively. The survival rate of all mice was also monitored for 42 d.

For in vivo localized dose-dense AC chemotherapy using implantable devices with the time-programmed pulsatile release, the AC devices designed to release DOX (5 mg/kg) and CYP (20 mg/kg) four times at different dose densities (120 h, 72 h, 24 h, and 0 h) were prepared. Tumor-bearing mice were randomly divided into five groups ($n = 6$): untreated, device-120 h, device-72 h, device-24 h and device-0 h. All mice's tumor volume, survival, and body weight were monitored

for 42 d. All animal experiments were performed according to protocols approved by the Institutional Animal Care and Use Committee of Ulsan National Institute of Science and Technology (UNISTIACUC-22–16).

2.7.　In vivo drug release study

We evaluated the amount of DOX and CYP released *in vivo* from devices for localized dose-dense AC chemotherapy. The devices were also implanted into the right flank of female BALB/c mice (6 weeks old), close to the hind limb. The implanted devices were removed from the mice at 3, 7, 14, 21 and 28 d after implantation to measure the DOX and CYP remaining in the device. DOX and CYP remaining in the device were measured using UV–vis spectrophotometry at 479 nm and 210 nm after dissolution in PBS.

2.8.　Bioluminescence imaging

For *in vivo* bioluminescence imaging (BLI), 4T1-Luc2 tumor-bearing mice were anesthetized with 1.5%−2% isoflurane and injected intraperitoneally with 150 mg/kg D-luciferin. The mice were imaged 12 min after injection. Harvested tumors and major organs, including heart, lung, liver, kidney and spleen, were immersed into 15 mg/ml D-luciferin in DPBS for *ex vivo* BLI. *In vivo* and *ex vivo* BLI was performed using an *in vivo* optical and X-ray imaging system (In-Vivo Xtreme; Bruker). Images were analyzed using Molecular Imaging (MI) software (version 7.5.2; Bruker).

2.9.　Histological analysis

Harvested tumors and major organs were fixed in a 4% paraformaldehyde solution. Fixed tissues were processed for paraffin embedding, and 4 μm-thick tissue sections were prepared. The sections were deparaffinized using xylene and rehydrated through a series of ethanol solutions (100%, 90%, 80% and 70%). Hematoxylin and eosin (H&E) staining was performed to observe general tissue morphology. Terminal deoxynucleotidyl transferase-mediated dUTP biotin nick end labeling (TUNEL) staining was performed using a TUNEL assay kit (ab206386; Abcam, Cambridge, MA, USA) to detect apoptotic tumor cells according to the manufacturer's protocol. Immunohistochemical (IHC) assays were performed on tumor sections to evaluate the expression of cell proliferation marker (Ki67) and drug resistance-associated membrane proteins (P-glycoprotein and BCRP/ABCG2). To detect Ki67, we used rabbit monoclonal anti-Ki67 (ab16667; Abcam, Cambridge, UK) at a dilution of 1:200, followed by incubation with a donkey anti-rabbit IgG H&L secondary antibody with Alexa Fluor 488 (1:1,000, ab150073; Abcam). Rabbit monoclonal anti-P-glycoprotein (1:1200, ab170904; Abcam) was used for P-glycoprotein staining, while rabbit monoclonal anti-BCRP/ABCG2 (ab207732; Abcam) at a dilution of 1:4000 was used for BCRP/ABCG2 staining. These sections were incubated with a goat anti-rabbit IgG H&L secondary antibody with Alexa Fluor 568 (1:1,000, ab175471; Abcam). DAPI was used to stain the nuclei of the sectioned tumors. Each section was quantified using Qupath software after imaging.

2.10.　Western blot analysis

Portions of frozen tumor tissues were homogenized in radioimmunoprecipitation assay (RIPA) buffer (RC2002–050–00; Biosesang, Seongnam, Republic of Korea) supplemented with a protease inhibitor cocktail (BPI-9200; Tech & Innovation™, Bucheon, Korea). The samples were centrifuged at 16,000 xg for 20 min at 4 °C. Supernatants were collected, and their protein concentrations were determined using the Pierce™ BCA protein assay kit (23,227; Thermo Fisher Scientific). Proteins were separated using SDS-PAGE and transferred to polyvinylidene fluoride (PVDF) membranes. The transferred membranes were blocked using EveryBlot Blocking Buffer (12,010,947; Bio-Rad, Hercules, CA, USA) for 5 min at room temperature. After blocking, membranes were incubated for 2 h with primary antibodies, including rabbit monoclonal anti-P-glycoprotein antibody (1:5,000, ab170904; Abcam) and rabbit monoclonal anti-BCRP/ABCG2 (1:1,000, ab207732; Abcam) at 4 °C. Following three 10-min washes with TBS-T, the membrane was incubated for 1 h with secondary antibodies, goat anti-rabbit IgG ($H + L$)-HRP (1:5000, SA002–500; GenDEPOT, Houston, TX, USA) at room temperature. The protein stripes were visualized by Clarity™ Western ECL substrate (1,705,061; Bio-Rad). The band intensity of target protein expression was quantified using ImageJ software. The expression of target proteins was normalized to a housekeeping gene expression.

2.11.　Statistical analysis

The data were presented as mean $\pm$ standard deviation. Statistical significance was assessed using a one-way analysis of variance (ANOVA) followed by Tukey's multiple comparison test. The analysis used GraphPad Prism 9 software (GraphPad Software Inc.). A *P*-value of less than 0.05 was considered statistically significant.

3.　Results and discussion

3.1.　Preparation and characterization of 3D printed devices for local dose-dense chemotherapy

We used extrusion 3D printing techniques to fabricate devices for dose-dense chemotherapy utilizing local delivery. The devices were designed as capsule structures with cylindrical PCL shells containing DOX and CYP mixed PF127 gels. (Fig. 2A). PF127 gel exhibited suitable rheological properties for extrusion-based printing and shape retention at 21 °C (Fig. S1). PCL and drug-loaded PF127 gels were printed with pneumatic extruders according to three different printing layer designs (outlet layer, drug layer and porous layer) that comprise the device devised through the visualized motion program. The outlet layer is located on the end face of the capsule and has a 250 μm diameter hole in the center to allow the drug inside the device to release outward. The drug layer contains a 30% (w/v) PF127 hydrogel mixed with drugs, and gels with different types and concentrations of drugs can be applied to fabricate this layer for various treatments. We also modified the design of the drug layer and the porous layer in between to control the
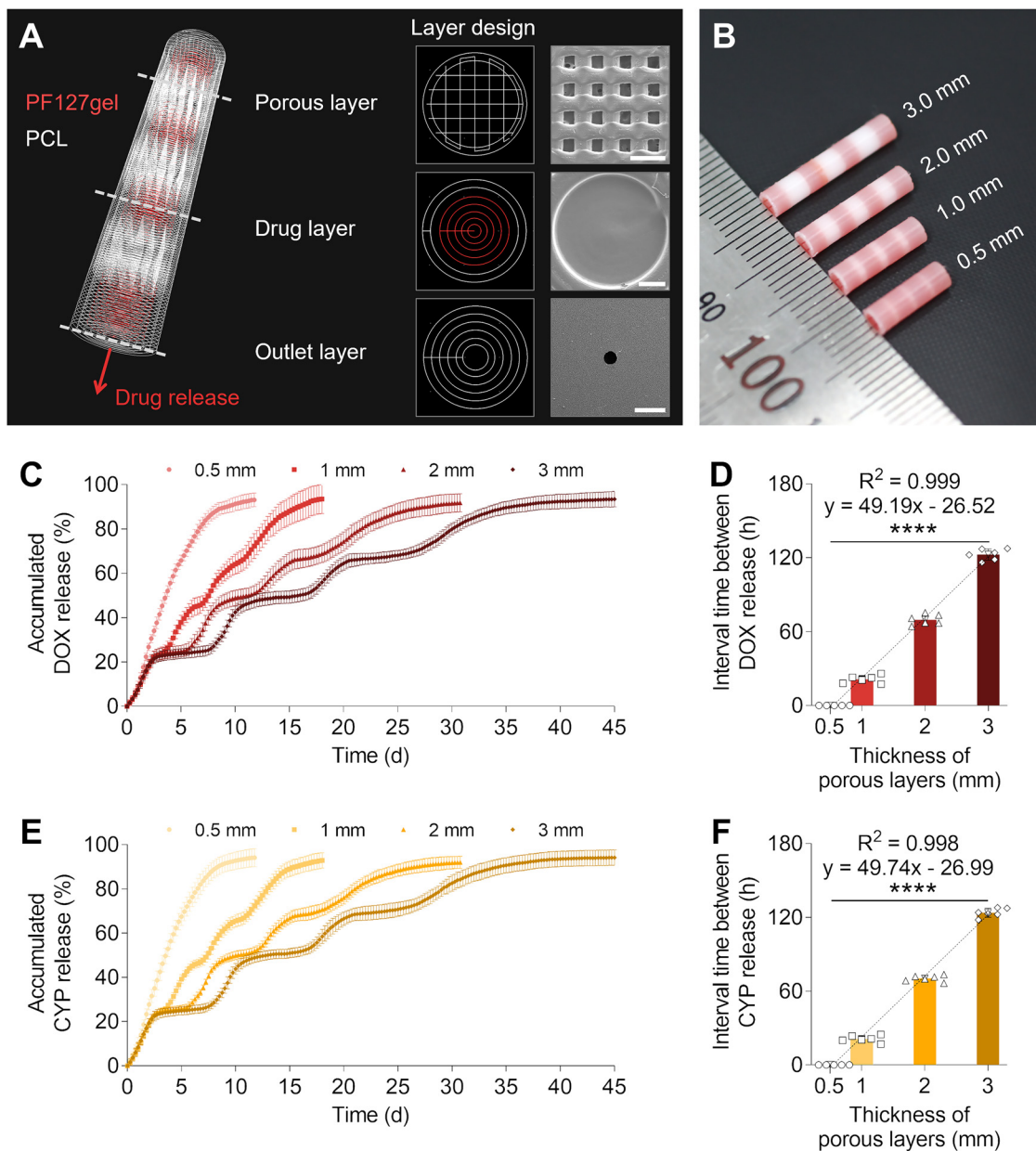
Fig. 2 – Characterization of 3D printed devices with programmable pulsatile release profile to control dose density. (A) Visualized motion program and SEM images of the 3D printed device composed of porous, drug, and outlet layers (Scale bar: 500 μm). (B) Optical image of a capsule device with various porous layer thicknesses. (C-F) *In vitro* DOX and CYP release properties of 3D printed devices with various thicknesses of porous layers: (C and E) Release kinetics of (C) DOX and (E) CYP. (D and F) the interval time between drug releases of (D) DOX and (F) CYP. All data are shown as means ± SD (*n* = 6). ****P< 0.0001.

device's internal structure to modulate the pharmacokinetic properties. In particular, the number of drug layers can be adjusted to control the number of drug releases, as previously described in our work [40]. From fabricating the capsules to implanting them into the body, the 30% (w/v) PF127 hydrogels in the drug layers were thermally cross-linked to maintain the printed space without migration into adjacent porous layers. We employed FE-SEM to observe the surface morphology of the printed layers. In the SEM images of the outlet layer and porous layer printed according to the design, the drug release

outlet with a diameter of 250 μm and a porous surface with a total pore area of 0.392 mm^2 were observed, respectively. In particular, the smooth surface of the drug-mixed PF127 gel was observed in the SEM images of the drug layer, which validated that DOX and CYP were well solubilized in the PF127 hydrogel. We fabricated various 3D printed devices with different designs for each experiment to realize local dose-dense chemotherapy (Table S1). For example, by varying the thickness of the porous layer from 0.5 mm to 1.0 mm, 2.0 mm and 3.0 mm, AC devices with different internal structures were

fabricated for local dose-dense AC chemotherapy in syngeneic TNBC mouse models (Fig. 2B).

3.2.   In vitro *drug release properties*

For dose-dense chemotherapy utilizing local delivery, the implantable device can control a key parameter, dose density, by adjusting the time interval between drug releases. Our previous work on 3D printed device development has validated that increasing the thickness of a device's porous layer can increase the time interval between drug release pulses [40]. Leveraging this advantage, we evaluated the release kinetics of DOX and CYP in 3D printed devices with different porous layer thicknesses to validate the ability to modify the dose density of the device for a dose-dense AC regimen. To investigate the *in vitro* drug release properties, we prepared 3D printed devices with various porous layer thicknesses (0.5, 1.0, 2.0, and 3.0 mm). These devices are designed to contain four drug gels to deliver the drug at the same number of times as the dose-dense AC regimen. In addition, the release properties of DOX and CYP from the devices were also monitored for up to 6 weeks, the treatment duration of the dose-dense AC therapy.

First, It was observed that as the porous layer thickness of the device decreased from 3.0 mm to 0.5 mm, the interval between DOX releases also decreased (Fig. 2C). Notably, DOX release in the form of four pulses, equal to the number of drug layers, was observed in the 1.0 mm, 2.0 mm, and 3.0 mm groups. However, the 0.5 mm group showed DOX release kinetics with no gaps between releases, and a linear release profile ($R^2 = 0.987$) was observed until the slope of the graph saturated after 80% drug release. Time intervals between releases of 21.3 ± 3.2 h, 69.8 ± 4.2 h and 122.6 ± 4.6 h were confirmed in the 1.0 mm, 2.0 mm and 3.0 mm groups, respectively. They showed that the time interval between DOX releases was linear, with increasing porous layer thickness verified ($R^2 = 0.999$; Fig. 2D). The duration of DOX release in each group increased as the time interval between releases increased (Fig. S2A). As the thickness of the porous layer increased from 0.5 mm to 1.0 mm, 2.0 mm and 3.0 mm, the time to 80% DOX release, the point at which the profile begins to saturate, increased linearly from 6.7 ± 0.5 d to 13.4 ± 1.8 d, 21.7 ± 1.3 d and 30.1 ± 0.8 d, respectively ($R^2 = 0.992$). As shown in Fig. 2E, the release profiles of CYP showed the same trend as DOX. The interval between CYP releases, which was not observed in the 0.5 mm group, increased with the porous layer's thickness to 1.0 mm (21.2 ± 2.7 h), 2.0 mm (70.3 ± 2.5 h) and 3.0 mm (123.8 ± 37 h) (Fig. 2F). Moreover, the time to 80% of CYP release increased consistently with increasing porous layer thickness from 6.5 ± 0.6 d to 29.2 ± 1.0 d ($R^2 = 0.992$) (Fig. S2B).

These results indicated that the desired time interval between the release of DOX and CYP could be realized by controlling the porous layer thickness of the device. Furthermore, our device showed high encapsulation efficiency of DOX and CYP with $91.86\% \pm 2.81\%$ and $92.91\% \pm 2.47\%$, respectively (Table S1). Our previous studies have demonstrated that the 3D printed device has the same pharmacokinetic properties regardless of *in vitro* and *in vivo* conditions, and similar *in vitro* drug release characteristics

were verified under pH 7.4 and slightly acidic (pH 6.5) conditions considering the tumor microenvironment [40]. Furthermore, the developed platform can release the drug at a desired concentration and duration depending on the device's internal design. For example, the duration of drug release can be expanded by increasing the thickness or number of drug layers in the device. Besides, the desired drug concentration can be realized by adjusting the concentration in the device's drug gel without changing the release characteristics. These results prove that our device with DOX and CYP can achieve suitable pharmacokinetic properties for local dose-dense AC chemotherapy to treat TNBC.

3.3.   In vitro *anti-cancer effect by controlling dose density of local chemotherapy*

We evaluated the *in vitro* anti-cancer effect of increasing the dose density of chemotherapy by utilizing 3D printed devices that can reduce the time interval between drug releases. Before the devices were applied, 4T1-Luc2 cells, murine TNBC cells, were cultured in 24-well plates overnight (Fig. 3A). DOX is an anti-cancer drug commonly used to treat TNBC and was prepared here as a model drug. As shown in Fig. 3B, we prepared devices that released DOX twice, with time intervals of 120 h, 72 h, 24 h and no interval (0 h) between releases. To evaluate the *in vitro* anti-cancer effect, the concentration of DOX in the device was also adjusted to 0.01%, 0.05% and 0.10% (w/v). These devices were placed on top of PCL mesh supports to prevent them from touching the bottom of the well plate and limiting the space for the cells to grow. During the 9 d incubation period, the culture medium was changed daily to prevent the accumulation of DOX released from the device into the media inside the wells. On Day 9, at the end of the release, the devices and supports were removed and replaced with fresh culture medium and allowed to recover for 24 h.

To determine cell viability in response to reduced DOX release intervals utilizing 3D printed devices, we performed a live/dead cell viability assay with our samples (Fig. 3C). The number of live cells in the fluorescence images of each group was counted using Qupath software. First, the *in vitro* anti-cancer effect of dose density variation was verified by utilizing devices with the same DOX concentration but different release time intervals. The groups treated with the 0.01% (w/v) DOX device showed a significantly reduced number of live cells than the untreated group ($P < 0.0001$). The number of live cells in the 72 h, 24 h, 120 h and 0 h groups was 42.28%, 43.29%, 50.54% and 66.08% of the untreated group, respectively (Fig. 3D). This result demonstrated that increasing the dose density from 120 to 24 and 72 h effectively enhances the *in vitro* anti-cancer effect. However, the 0 h group, which has the highest dose density and where DOX release ends first, showed the largest number of live cells than other device groups. This result was influenced by the growth of surviving 4T1-Luc2 cells even after finished DOX release in the 0 h group. It was also associated with a lower anti-cancer effect in the 24 h group than in the 72 h group. We applied devices with increasing DOX concentrations of 0.05% and 0.10% (w/v) to validate the trend change in dose density with increasing concentrations of DOX. As the concentration of DOX in the device increased from 0.01% to 0.05% and 0.10%
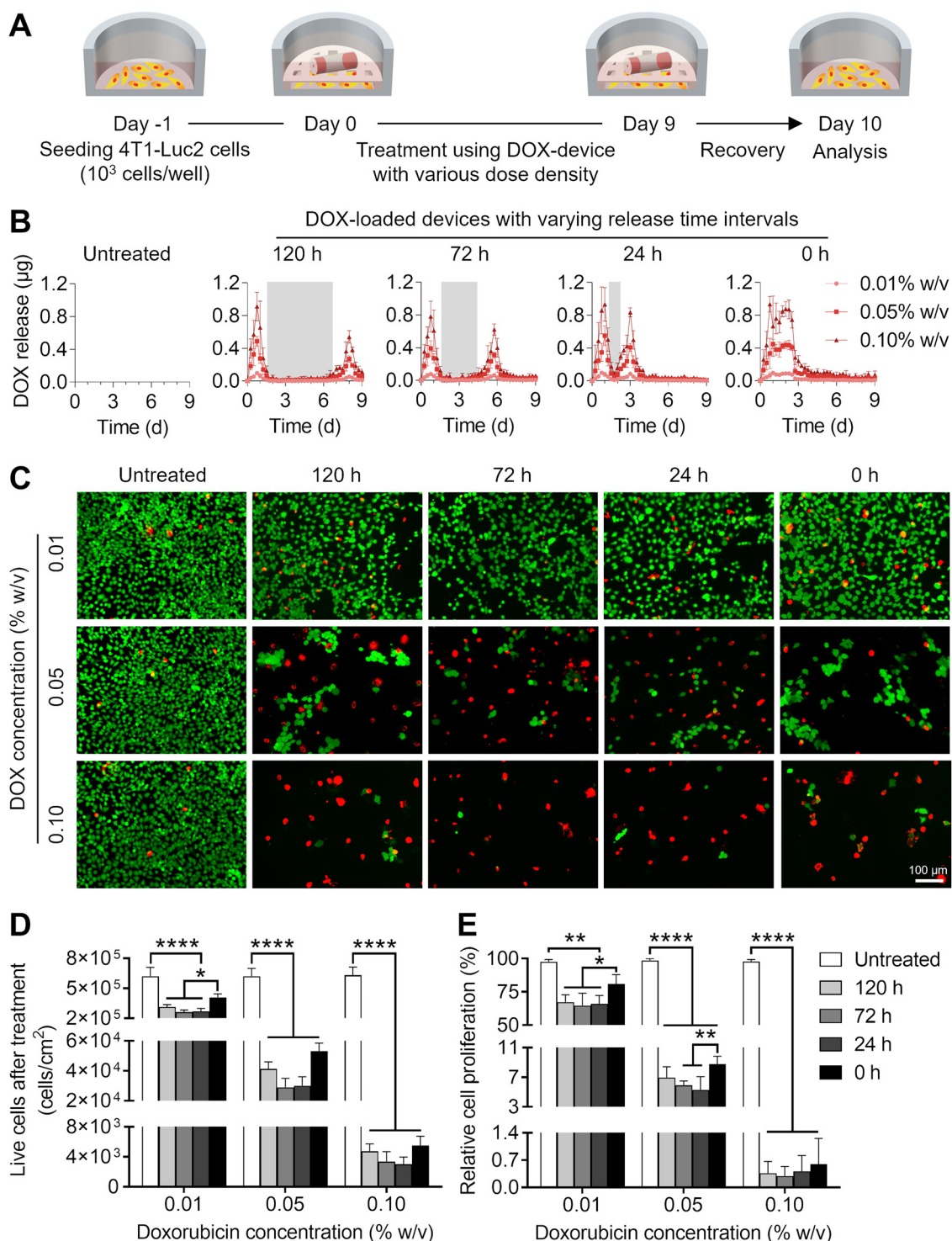
Fig. 3 – *In vitro* anti-cancer effect of controlling dose density using DOX-loaded devices. **(A)** A timeline describing the *in vitro* cytotoxicity experiment using 4T1-Luc2 cells and 3D printed devices with various dose densities. **(B)** DOX release profile of devices with different dose densities for *in vitro* cytotoxicity test (gray areas: the interval between drug release). **(C)** Fluorescence images of live/dead assay of 4T1-Luc2 cells cultured 10 d after treatment (Scale bar: 100 μm). **(D)** Quantification of live cells after the respective treatments. **(E)** The relative proliferation of 4T1-Luc2 cells with capsular devices with different dose densities and DOX concentrations. All data are shown as means ± SD ($n = 6$). *$P < 0.05$, **$P < 0.01$, ****$P < 0.0001$.

(w/v), the number of viable cells in all groups decreased rapidly to 4.64%–8.57% and 0.48%–0.89%, respectively, compared to the untreated group. The trend in cell viability between groups with different release time intervals but the same concentration of DOX was similar as the DOX concentration increased. The relative cell proliferation rate of each group according to the release interval and concentration change of DOX was also evaluated by alamarBlue assay. As shown in Fig. 3E, this result showed a similar tendency to the live cell counting result. Furthermore, the drug-free device's relative cell proliferation rate was similar to the untreated group validated by the alamarblue assay using a human TNBC cell line and a human mammary epithelial cell line, as the previous study described [40].

From these results, we verified that the anti-cancer effect could be improved by increasing the dose density of dose-dense chemotherapy to a certain level by controlling the release interval of the anti-cancer drug with 3D printed devices. When the number of drug releases is fixed, an excessive reduction in the release time interval to increase the dose density reduces the exposure time of the anti-cancer drug to the cancer cells. In this case, residual cells will grow after treatment, reducing the anti-cancer effect. Thus, optimization of dose density should be considered for high anti-cancer effectiveness. Besides, higher concentrations of anti-cancer drugs may be considered for dose-dense chemotherapy to increase the anti-cancer effect. Therefore, we implemented dose-dense chemotherapy using a 3D printed device under *in vitro* conditions and confirmed the feasibility of applying more effective TNBC treatment through dose density modulation.

3.4. *In vivo anti-cancer effect of controlling dose density of local chemotherapy in syngeneic TNBC mouse model*

To verify the effect of increasing the dose density of dose-dense chemotherapy using the implantable device on the *in vivo* anti-cancer effect, we evaluated the therapeutic efficiency in a syngeneic TNBC mouse model. The syngeneic TNBC models were prepared by orthotopic injection of 4T1-Luc2 cells into female BALB/c mice (Fig. 4A). It shows similar characteristics to TNBC patients, as tumors grow faster and metastasize more easily than xenogeneic mouse models using human cell lines such as MDA-MB-231 [44]. In particular, the orthotopic TNBC model made with 4T1-Luc2, a luciferase-expressing cell line, can measure luminescence signals with *in vivo* BLI, allowing tumor growth to be monitored during treatment. To increase the dose density of local chemotherapy, groups with 120 h, 72 h, 24 h and 0 h release intervals were prepared by reducing the length of the porous layer of devices designed to release 5 mg/kg DOX five times (Fig. S3). These devices showed *in vivo* DOX release results with similar trends to the *in vitro* experiments (Fig. S4). Although the *in vivo* release graphs did not show oscillations due to the low measurement frequency, similar release rates to the *in vitro* data were observed. To verify the anti-cancer effect of the device itself, a drug-free group was also prepared using devices made of PF127 hydrogel without drugs. Using a trocar, we implanted the prepared devices into 4T1-Luc2 tumor-bearing BALB/c mice (Fig. S5). An untreated group and an IT-72 h group with

five IT injections of 5 mg/kg DOX at 72 h intervals were also prepared for comparison. An IT injection is an administration method of the drug directly into the tumor and is often used as a positive control group to compare anti-cancer efficiency with LDDS [29]. In addition, this method has a higher anti-cancer effect than the intravenous injection used in clinical practice [23].

We monitored tumor volume, survival and weight changes in all groups over the 28 d treatment period (Fig. 4B-4D). Interestingly, among the groups implanted with DOX devices, the anti-cancer effect was enhanced in the device-24 h and device-72 h groups with higher dose density than the device-120 h group. As shown in Fig. 4B, the average tumor volume was reduced in the device-24 h (316.74 mm^3) and device-72 h (194.87 mm^3) groups compared to the device-120 h group (347.49 mm^3) on Day 28. In contrast, the 0 h group demonstrated the least effective tumor growth inhibition among the DOX-treated groups, with an average tumor volume of 464.81 mm^3. This observation aligns with the trend observed in the previous *in vitro* anti-cancer evaluation. After 60 d treatment, the survival rate among the DOX device groups was the highest in the device-72 h group, followed by device-24 h, device-120 h, and device-0 h (Fig. 4C). By comparing the device-72 h group and the IT-72 h group, both having the same dose density achieved through identical drug release or injection time intervals, it was observed that the average tumor volume in the device group (194.87 mm^3) was smaller than that in the IT group (276.77 mm^3), thereby validating the enhanced anti-cancer effect of DOX device. While all mice in the device group remained alive at the 40 d treatment, the IT injection group exhibited a survival rate of 0 at the same time point. Moreover, the average body weight of mice in all groups, except for the IT-72 h group, exhibited consistent increases throughout the treatment period, while the IT-72 h group showed consistent weight loss (Fig. 4D). It is related to the rapid absorption of DOX administered by IT injection within hours, as opposed to the group using devices without initial burst release characteristics [29]. From these results, it was demonstrated that dose-dense chemotherapy of TNBC utilizing the device had the enhanced anti-cancer effect than IT injection-based therapy, with less toxicity and higher anti-cancer efficiency. In addition, the drug-free group's tumor growth, survival rate, and body weight change showed similar trends to those of the untreated group. It indicated that our device, made of commercially available biodegradable materials, has no anti-cancer effect or toxic reaction. Through *in vivo* BLI, the tumor growth of 4T1-Luc2 tumor-bearing mice in each group was monitored and quantitatively measured through bioluminescence detection (Fig. 4E and S6). The results verified a similar trend as the previous tumor volume measurements. This tendency was also observed when comparing the size of harvested tumors among all groups at day 28 (Fig. 4F).

As shown in Fig. 4G, histological analysis was performed on tumor tissue sections from all groups. After analyzing the H&E-stained images of each group, the largest area of damaged tissue was observed in the device-72 h group. Then, the damaged tissue area decreased from the IT-72 h group to device-24 h, device-120 h, and device-0 h groups
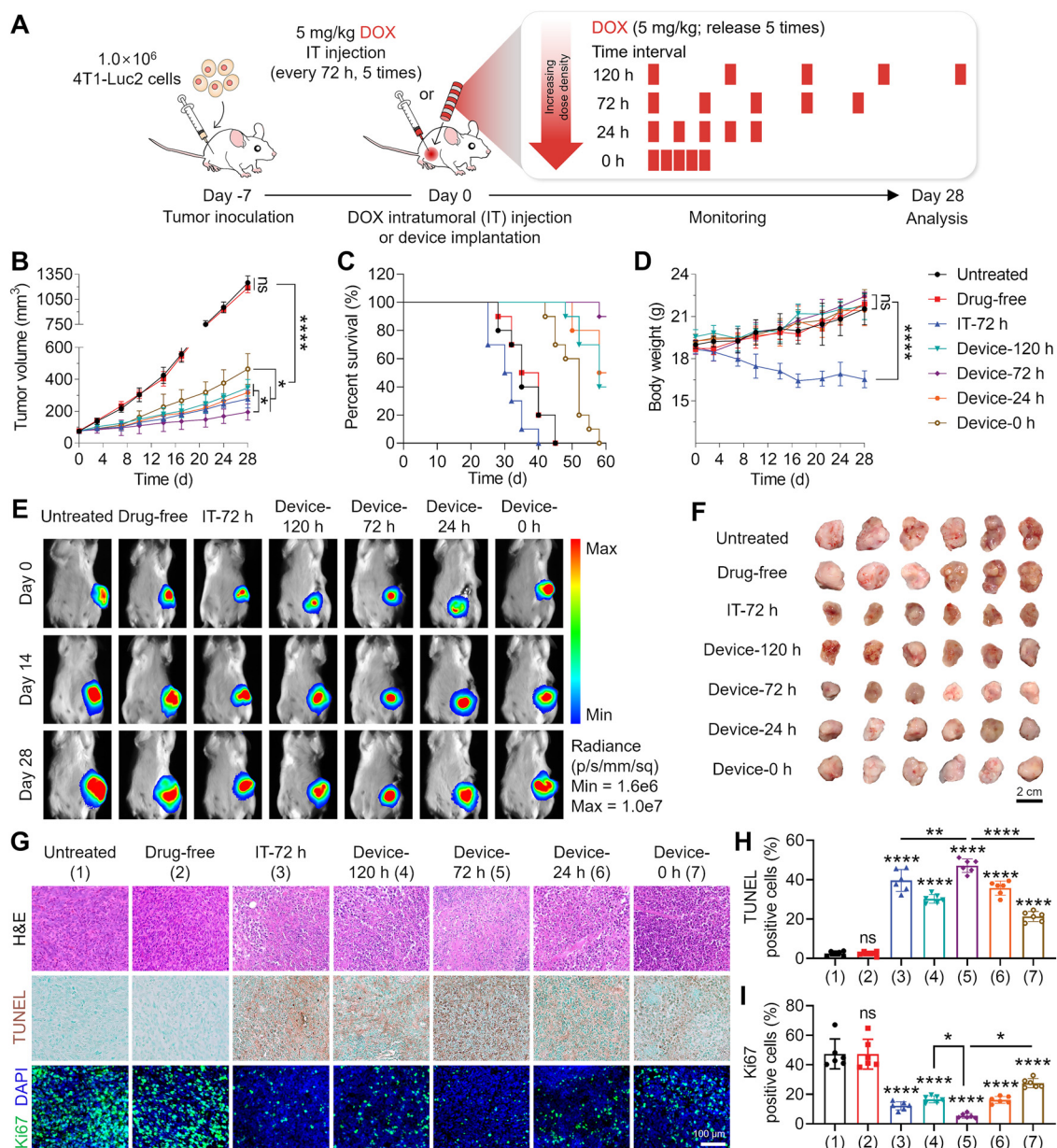
Fig. 4 – *In vivo* anti-cancer effect according to control dose density of DOX-loaded devices in syngeneic TNBC mouse models. (A) Schematic illustration of the *in vivo* experimental procedure: preparation of an orthotopic TNBC model using 4T1-Luc2 cells and implantation of dose density-controlled DOX devices. (B) Tumor growth ($n = 6$), (C) survival rates ($n = 10$), and (D) body weights of treated mice ($n = 6$). (E) *In vivo* bioluminescence images to track the growth of tumor cells after various treatments applied on primary orthotopic TNBC tumors. (F) Optical images of harvested tumors from each group. (G) Representative H&E and immunohistochemical (TUNEL, Ki67) staining results of tumor sections at day 28 after device implantation (Scale bar: 100 μm). (H and I) Quantitative analysis of (H) apoptotic and (I) proliferative cells in the harvested TNBC tumors according to data in (G) ($n = 6$). All data are shown as means ± SD. *$P < 0.05$, **$P < 0.01$, ****$P < 0.0001$.

in order. In contrast, minimal tissue damage was observed in the tumor tissue sections of the untreated and drug-free groups. Consistent findings were observed in the TUNEL staining results, indicating the presence of apoptotic cells in tumor tissue sections. The tumor section images of each group were quantitatively analyzed for TUNEL-positive cells using Qupath software (Fig. 4H). The highest percentage

of apoptotic cells was found in the device-72 h group at 47.08% ± 3.42%. The proportion of TUNEL-positive cells in tumor sections decreased in the following order: IT-72 h (39.64% ± 5.56%), device-24 h (35.77% ± 3.59%), device-120 h (30.26% ± 2.22%), device-0 h group (21.31% ± 2.53%). In contrast, the drug-free and untreated groups had relatively low percentages of apoptotic cells, 2.52% ± 1.08% and 2.49%

± 1.23%, respectively. In clinical practice, the level of Ki67 expression is an important factor in determining tumor aggressiveness [45]. Ki67 immunostaining was performed to detect proliferative cells and analyze the aggressiveness of the tumor tissues of each group. Quantification revealed high Ki67 expression of 47.34% ± 10.10% and 47.18% ± 10.16% of tumor sections in the untreated and drug-free groups (Fig. 4I). The proportion of Ki67-positive cells in the tumor tissues decreased in the order of device-0 h (27.54% ± 3.12%), device-120 h (16.64% ± 2.35%), device-24 h (16.24% ± 2.34%), IT-72 h (12.23% ± 2.76%), and device-72 h groups (5.43% ± 1.60%). This sequence is reversed to that of the TUNEL assay. These results show that local dose-dense chemotherapy using an implantable device and its dose density control effectively increase anti-cancer efficiency in the syngeneic TNBC model. It also supports the results of *in vitro* experiments that proper regulation of dose density is essential to maximize anti-cancer effects. Notably, the treatment using the device showed a greater reduction in tumor growth compared to the IT injection method, another local delivery approach with an equivalent dose, number of doses, and dosing intervals. Furthermore, no adverse effects were observed, highlighting its significant clinical advantages. In addition, our device allows for minimally invasive implantation using the trocar, which has the potential to provide a therapeutic option for breast cancer patients who are unwilling to undergo surgical breast removal.

3.5. In vivo *anti-cancer efficacy of dose-dense AC regimen using IT injection*

For local chemotherapy using an implantable device that mimics the dose-dense AC regimen preferred for TNBC treatment, we first verified the anti-cancer effect of the dose-dense AC regimen and its dose density control using IT injection, a conventional local administration method (Fig. S7A). For our experiments, we considered the doses of DOX and CYP used to treat TNBC in the clinic. The dose-dense AC regimen for TNBC patients consists of 60 mg/m^2 (1.62 mg/kg) DOX and 600 mg/m^2 (16.2 mg/kg) CYP administered intravenously for a total of four doses [46]. The DOX and CYP doses for humans are equivalent to the mouse dose of 20 mg/kg of DOX and 200 mg/kg of CYP [47]. However, these doses were set for systemic administration, so lower doses of 5 mg/kg DOX and 20 mg/kg CYP were considered for our experiments using local delivery. To assess the anti-cancer efficacy of AC regimens using IT injection, we conducted experiments using the 4T1-Luc2 TNBC mouse model. The study included the following groups: DOX-168 h, CYP-168 h, and AC-168 h, where 5 mg/kg DOX, 20 mg/kg CYP and their combination, respectively, were IT injected at 168 h intervals. Additionally, we investigated the impact of dose density variations by including the AC-168 h and AC-240 h groups, which received the same dose as the AC-72 h group but with dosing intervals changed to 72 h and 240 h, respectively. As a negative control, a group receiving IT injections of PBS at 168 h intervals was included for comparison. All drugs were administrated four times, the same number of times as clinically, at set time intervals.

Changes in the tumor volume of the treated mice were monitored until Day 42, the same as the clinical treatment period (Fig. S7B). Enhanced tumor growth inhibition was seen in the AC-168 h group compared to the DOX-168 h and CYP-168 h groups at the same dosing time interval. The average tumor volume at day 42 of treatment was 567.57 mm^3 and 709.27 mm^3 for the DOX-168 h and CYP-168 h groups, respectively, while the AC-168 h group had a smaller tumor volume of 432.29 mm^3 than the previous two groups. This result indicates that AC, a combination of DOX and CYP, has an enhanced anti-cancer effect due to the synergy of the two drugs. These values are significantly lower than the PBS-168 h group, which had an average tumor volume of 1948.06 mm^3 on Day 42. Furthermore, the IT injected AC groups gradually reduced average tumor volume as the dose density increased from 240 h to 168 h and 72 h, with tumor volumes recorded as 527.96 mm^3, 432.29 mm^3 and 374.15 mm^3, respectively. The results prove that a dose-dense AC regimen utilizing local delivery inhibits tumor growth effectively. Survival rates and body weight changes of mice in all groups were also monitored (Fig. S7C and S7D). As shown in Fig. S7C, we observed a correlation between the survival rate of the groups and the average tumor volume, indicating an inverse relationship. For instance, the PBS-168 h group, with the largest average tumor volume, exhibited the lowest survival rate of 0 at Day 45. Conversely, the AC-72 h group, which demonstrated the highest tumor growth inhibition, had a lower survival rate than the CYP-168 h group. This phenomenon can be attributed to toxic reactions from excessively dense drug administration. Due to the toxicity of the drugs administered by IT injection, all treated groups had lower body weights than the PBS-168 h group at Day 42 (Fig. S7D). Among the groups dosed at 168 h intervals, the AC-168 h group had the lowest body weight, followed by the DOX-168 h and CYP-168 h groups. Interestingly, the body weight of mice decreased as the dose density of the dose-dense AC regimen using IT injection increased from 240 h to 168 h and 72 h. During the treatment period, the tumor growth of mice was detected in all groups by *in vivo* BLI (Fig. S7E and S7F). Quantification of the bioluminescence signal detected over 42 d observed the same trend as the previous results for the average tumor volume changes (Fig. S7E). We determined the occurrence of TNBC metastasis by the bioluminescence signal detected in mouse areas other than the primary tumor. On Day 28 of treatment, mice with metastases were identified in the PBS-168 h and CYP-168 h groups (Fig. S7F). On day 42, metastases were found in all groups of mice. For enhancing anti-cancer efficiency, the reduction of side effects such as toxicity and the increase of anti-cancer effects should be considered simultaneously. These results demonstrate the effectiveness of increasing the dose density of local dose-dense AC chemotherapy through IT injection in reducing tumor volume. However, the observed side effects, such as poor survival rate and weight loss, pose challenges for its clinical application as a treatment option. Previous experiments have shown enhanced anti-cancer effects and minor side effects in mice implanted with DOX devices compared to mice injected with DOX at the same drug dosing interval. Therefore, the 3D printed device is necessary to develop local dose-dense AC chemotherapy for treating TNBC with high anti-cancer efficiency.

3.6. In vivo *anti-cancer efficacy of local dose-dense AC regimen using 3D printed devices*

To evaluate the anti-cancer efficiency of local dose-dense AC chemotherapy using a 3D printed device with increasing dose density, we implanted AC devices with 120 h, 72 h, 24 h, and 0 h release intervals into a syngeneic TNBC model (Fig. 5A). The implanted devices were designed to release 4 times the same dose of 5 mg/kg DOX and 20 mg/kg CYP as in the previous IT injection experiment. These devices showed *in vivo* DOX and CYP drug release results with similar release rates in the *in vitro* experiments (Fig. S8). The devices were

positioned to contact the tumor in the syngeneic TNBC model via a trocar. In addition, an untreated group was prepared as a negative control for comparison. We monitored the average tumor volume of all groups until day 42 (Fig. 5B). The 72 h group, which had a higher dose density than the 120 h group, exhibited the most effective tumor growth inhibition. The average tumor volume in the 72 h group was 292.77 mm^3, smaller than that of the IT injection group (374.15 mm^3) with the same administration time interval, dose, and frequency (Fig. S7B). Next, tumor volume changes with dose density modulation were identified in the following order: 24 h group (420.99 mm^3), 120 h group (524.41 mm^3),
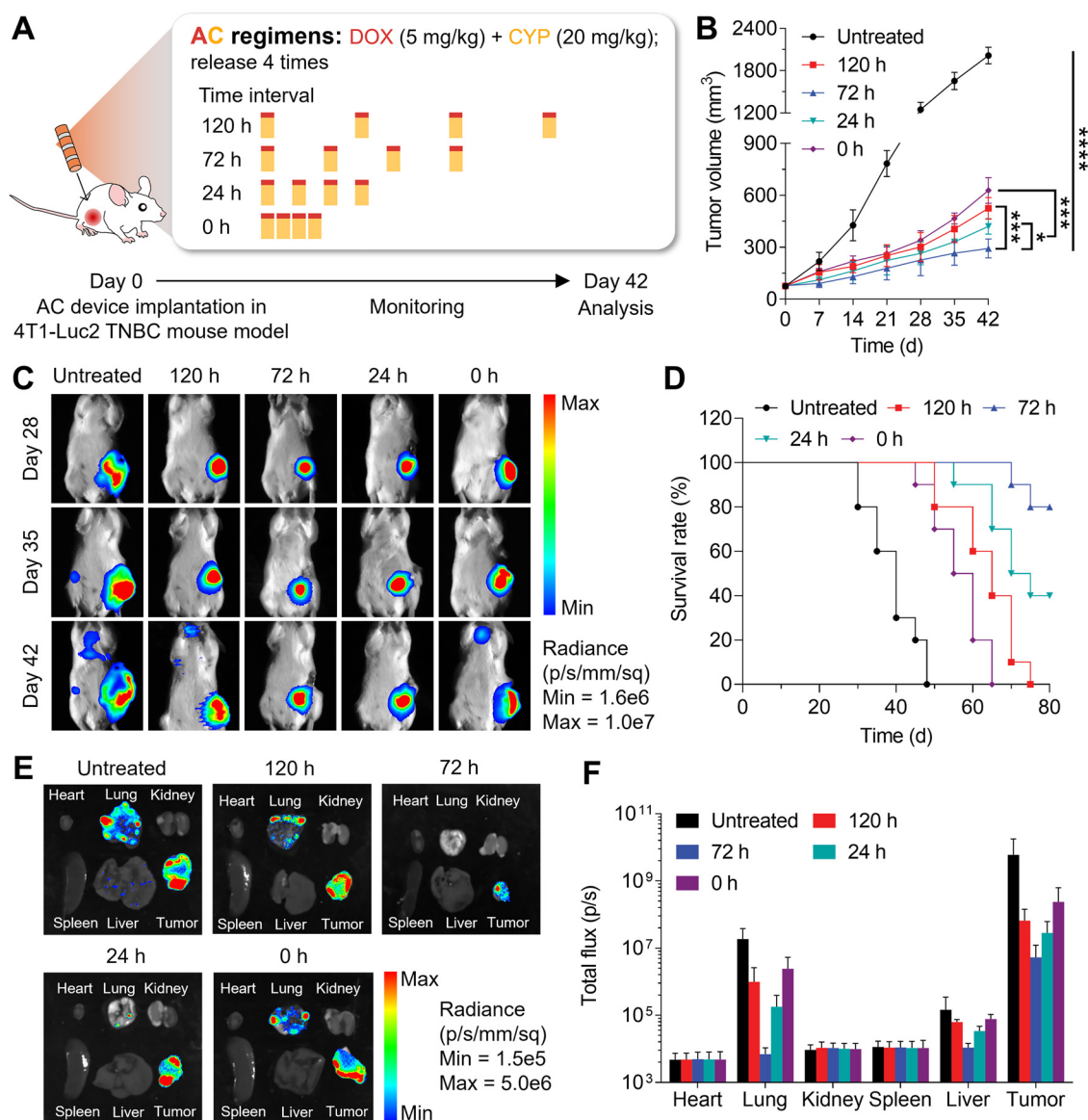
Fig. 5 – Local dose-dense AC chemotherapy using 3D printed devices in syngeneic TNBC mouse models. (A) A schematic diagram of the *in vivo* experimental procedure for local dose-dense AC chemotherapy using the 3D printed device. **(B)** Changes in tumor volume of treated mice at 42 d (*n* = 6). **(C)** *In vivo* bioluminescence images to track the spreading and growth of tumor cells after localized dose-dense AC chemotherapy. **(D)** Survival rates of treated mice (*n* = 10). **(E)** *Ex vivo* bioluminescence images of harvested tumors and major organs from each group. **(F)** The total flux of bioluminescence of their harvested tumor and major organs after local dose-dense AC chemotherapy (*n* = 6). All data are shown as means ± SD. *$P < 0.05$, *** $P < 0.001$, ****$P < 0.0001$.

and 0 h group (627.95 mm^3). Notably, the 0 h group, which had the shortest duration of drug release among all the groups using the device, exhibited the worst tumor growth inhibition. These results indicate a sufficient drug release period for effective tumor growth inhibition. In contrast, the untreated group demonstrated a significantly larger average tumor volume of 2014.69 mm^3 compared to those treated with the device. Moreover, *in vivo* BLI was performed to monitor tumor growth during the treatment period (Fig. 5C). There was a consistent correlation between the change in bioluminescence signal intensity and the corresponding variation in tumor volume over time (Fig. S9). On Day 42, a region of reduced luminescence signal was observed in the center of the tumor in the untreated group. This phenomenon seems to be an effect of central necrosis due to excessive tumor size increase. Besides, survival rates and body weight changes in all groups were monitored. For 80 d, the 72 h group indicated the highest survival rate, with a clear correlation between higher survival rates and smaller average tumor volumes (Fig. 5D). The untreated group exhibited the lowest survival rate, with all mice dying on day 48, followed by the 0 h group and the 120 h group, where all mice died on Day 65 and 75, respectively. In the IT injection group under the same dosing conditions, 30% survival was seen at day 60 of treatment in the device group, and 100% and 80% survival were found at 60 d and 80 d, respectively (Fig. S7C). In contrast to dose-dense AC therapy utilizing IT injection, mice implanted with AC devices consistently gained weight throughout the treatment period, the same as the untreated group (Fig. S10). From these results, we proved that local dose-dense AC chemotherapy using a 3D printed device was implemented for TNBC treatment. This treatment using an implantable device was confirmed to have enhanced anti-cancer efficacy compared to treatment using IT injection under the same treatment conditions. The anti-cancer effect of local dose-dense AC chemotherapy changed with the adjustment of dose density, underscoring the importance of optimizing dose density for achieving maximum anti-cancer efficacy in this therapy. Furthermore, exploring modifications in drug dosage, selection, combinations, treatment frequency, and other parameters can be considered to enhance the anti-cancer effectiveness of the developed therapy.

3.7. Anti-metastasis effects of local dose-dense AC regimen using 3D printed devices

The 4T1-Luc2 syngeneic TNBC model is well known to show aggressive tumor growth and metastasis similar to TNBC patients and is also used as a lung metastasis model [48]. We used this model to monitor metastasized cancer cells from the tumor to other organs during the treatment period by *in vivo* BLI. On Day 28, luminescence signals were detected only in the tumors of mice in all groups (Fig. 5C). On Day 35, a TNBC metastasis was identified in the left flank of a mouse with an anatomically located inguinal lymph node in the untreated group. On Day 42, luminescence signals were detected in the anatomical locations of mice's lung, thymus, axillary, and inguinal lymph nodes in the untreated, 120 h, and 0 h groups. In particular, the largest signal area was detected

in the mice in the untreated group. On Day 42, tumors and major organs, including heart, lung, kidney, spleen, and liver, were harvested from each mouse and analyzed by *ex vivo* BLI (Fig. 5E). In the 72 h group, no luminescence signal due to metastasis was found in major organs except the tumor. However, luminescence signals were detected in the lungs of all groups except the 72 h group, and the signal intensity increased in the order of 24 h, 120 h, 0 h, and untreated groups (Fig. 5F). In addition, metastasis was also found in the liver of the untreated group.

Metastatic foci were observed on the surface of the harvested lungs, and their sections were histologically analyzed to verify micrometastases (Fig. 6A). Among the treatment groups, the lowest number of metastatic foci was observed in the 72 h group (2.2 ± 1.0), and the number of metastatic foci increased in the order of 24 h (6.0 ± 1.3), 120 h (12.2 ± 1.6), and 0 h group (17.3 ± 1.9) (Fig. 6B). The untreated group had a significantly higher number of metastatic foci, 28.5 ± 5.7, than the other groups ($P < 0.0001$). We trained Qupath histopathology software to detect and quantify tumor areas metastasizing to the lungs. Whole lung sections from each group were quantitatively analyzed with Qupath software, and the smallest percentage of metastasis was identified in the 72 h group at 1.2% ± 0.3% (Fig. 6C). The percentage of metastatic tumors in whole lung sections increased in the order of 24 h (4.7% ± 0.5%), 120 h (16.0% ± 1.4%), 0 h (32.0% ± 1.5%), and untreated group (49.9% ± 6.2%). In the case of liver tissue, the software was able to detect and classify metastatic tumors and normal liver tissue as well as necrotic liver tissue in liver tissue sections (Fig. 6D). As shown in Fig. 6E, the number of metastatic foci on the liver surface increased in the order from 72 h (0.2 ± 0.4) to 24 h (4.0 ± 0.9), 120 h (7.5 ± 1.0), 0 h (8.8 ± 1.5), and untreated group (22.0 ± 3.9) in the same trend as the result of the lung. Necrotic liver tissue was also observed on the surface of the liver, especially in the untreated group. Furthermore, the metastasis rate in liver sections increased in the following order: 72 h (0.4% ± 0.4%), 24 h (6.8% ± 1.3%), 120 h (12.3% ± 1.6%), 0 h (16.1% ± 2.3%), and untreated group (38.0% ± 7.5%), with the same trend as the lung results (Fig. 6F). Additionally, organ sections, including the heart, spleen, and kidney, were analyzed, but no micrometastases were found (Fig. S11). These results showed that dose density control of local dose-dense AC chemotherapy using an implantable device effectively reduces metastasis of highly aggressive TNBC. In addition, the developed therapy can be used as adjuvant chemotherapy and applied together with radiation therapy and immunotherapy for enhanced therapeutic effects [49,50]. Instead of using chemotherapeutic drugs to induce cell apoptosis, our devices can also be equipped with immune adjuvants such as immune checkpoint blockade to disable the immune checkpoints of cancer cells and utilize immune cells to induce cancer cell death [51,52].

3.8. Drug resistance response of TNBC according to changes in dose density of local dose-dense AC therapy using 3D printed devices

Multidrug resistance (MDR) inhibits the ability of anti-cancer drugs to kill cancer cells and is a major factor in the failure
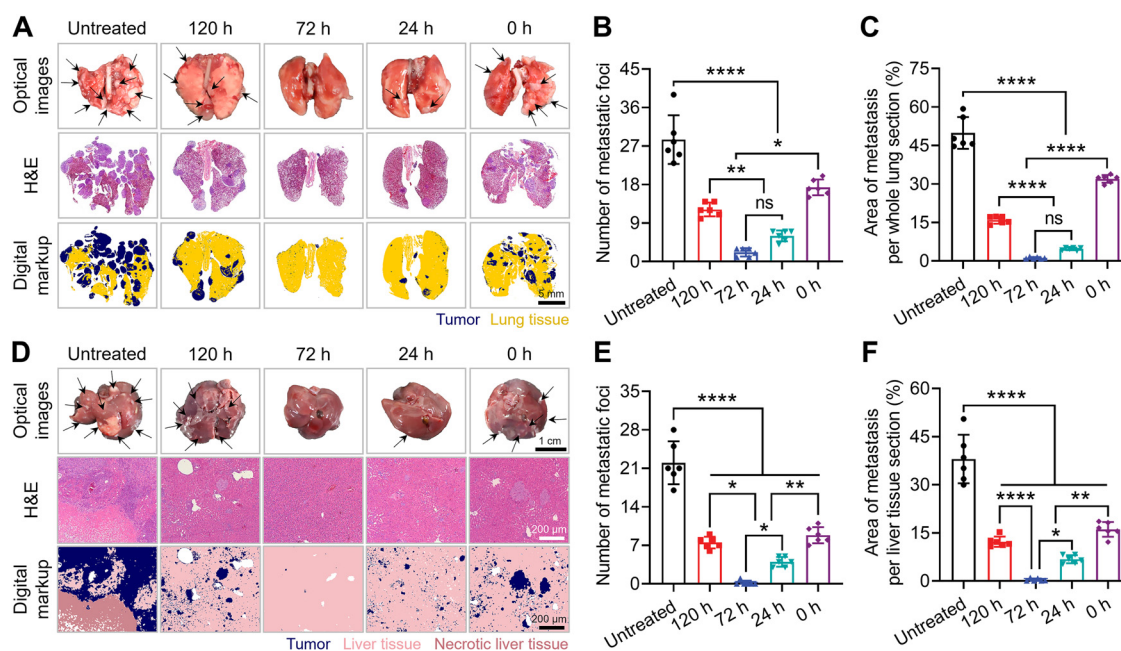
Fig. 6 – Lung and liver metastasis in syngeneic TNBC mouse models following dose density variation of local dose-dense AC therapy. (A and D) Representative optical images of (A) lungs and (D) livers, their H&E-stained sections, and digitally processed images to quantify metastatic tumor cells. (Scale bar: 5 mm). Black arrows point to metastatic tumors. (B and E) The number of metastatic foci on the (B) lung and (E) liver surface after treatment ($n = 6$). (C and F) Percentage of tumor area within (C) total lung area and (F) liver section after treatments ($n = 6$). All data are shown as means ± SD. *$P < 0.05$, **$P < 0.01$, ****$P < 0.0001$.

of chemotherapy [53]. MDR is associated with overexpression of ATP-binding cassette (ABC) transporter proteins, including P-glycoprotein (P-gp, ABCB1) and breast cancer resistance protein (BCRP, ABCG2), resulting in reduced accumulation of anti-cancer drugs in cancer cells [54]. To investigate the effect of increasing the dose density of local dose-dense AC chemotherapy utilizing an implantable device on the drug-resistant response of TNBC tumors, the expression of P-gp and BCRP in tumor tissues harvested on Day 42 of treatment was analyzed by western blot and IHC.

First, protein samples extracted from tumor tissues of each group were analyzed for the expression of P-gp and BCRP by western blot (Fig. 7A). Interestingly, higher expression of P-gp and BCRP was observed in the higher dose density groups. As the dose density increased in the order from the untreated group to the 120 h, 72 h, 24 h, and 0 h groups, P-gp/β-actin levels significantly increased to 0.28 ± 0.02, 0.77 ± 0.11, 1.54 ± 0.24, 2.48 ± 0.27, and 5.48 ± 0.33, respectively ($P = 0.005$; Fig. 7B). Compared to the untreated group, the 120 h, 72 h, 24 h and 0 h groups showed 2.7-fold, 5.5-fold, 8.8-fold, and 19.4-fold increased P-gp expression, respectively. Similarly, as the dose density increased from the untreated group to the 0 h group, BCRP/β-actin levels significantly increased by 0.29 ± 0.02, 0.73 ± 0.07, 1.46 ± 0.14, 2.26 ± 0.17, and 4.15 ± 0.18 ($P < 0.0001$; Fig. 7C). From the 120 h group to the 0 h group, increasing dose density resulted in 2.5-fold, 5-fold, 7.8-fold, and 14.4-fold higher expression of BCRP compared to the untreated group.

IHC analysis was performed to examine the expression of P-gp and BCRP in the tumor sections of each group. According to the fluorescence microscopy images, as the dose density increased from the untreated group to the 0 h group, the expression levels of P-gp and BCRP increased (Fig. 7D). The P-gp positive area in tumor section images was quantified with Qupath software (Fig. 7E). As a result, the highest expression of P-gp was shown in the 0 h group ($35.95\% \pm 4.12\%$) with the highest dose density. Then, as the dose density decreased, the P-gp positive area decreased in the order of 24 h ($15.19\% \pm 2.64\%$), 72 h ($7.58\% \pm 1.85\%$), and 120 h groups ($5.24\% \pm 1.35\%$). The P-gp expression was hardly observed in the untreated group ($0.33\% \pm 0.26\%$). Similarly, the BCRP positive area was also quantitatively analyzed. The BCRP expression area increased as the dose density increased in the order of untreated ($1.52\% \pm 1.02\%$), 120 h ($6.91\% \pm 2.12\%$), 72 h ($8.97\% \pm 2.09\%$), 24 h ($17.10\% \pm 2.08\%$), and 0 h groups ($33.84\% \pm 4.92\%$) (Fig. 7F).

We demonstrated that the excessively high dose density of local dose-dense AC chemotherapy using implantable devices could inhibit the anti-cancer effect by increasing the drug resistance response of tumors. These results support the reduced inhibition of tumor growth and metastasis in the 0 h and 24 h groups, which had higher dose densities than the 72 h group in the previous experiments. Localized drug delivery systems for chemotherapy have been recognized for their superior anti-cancer effectiveness. However, there have been concerns regarding prolonged drug release potentially leading to tumor drug resistance and reducing treatment efficacy. However, our device effectively reduced drug resistance responses by increasing the interval between drug release
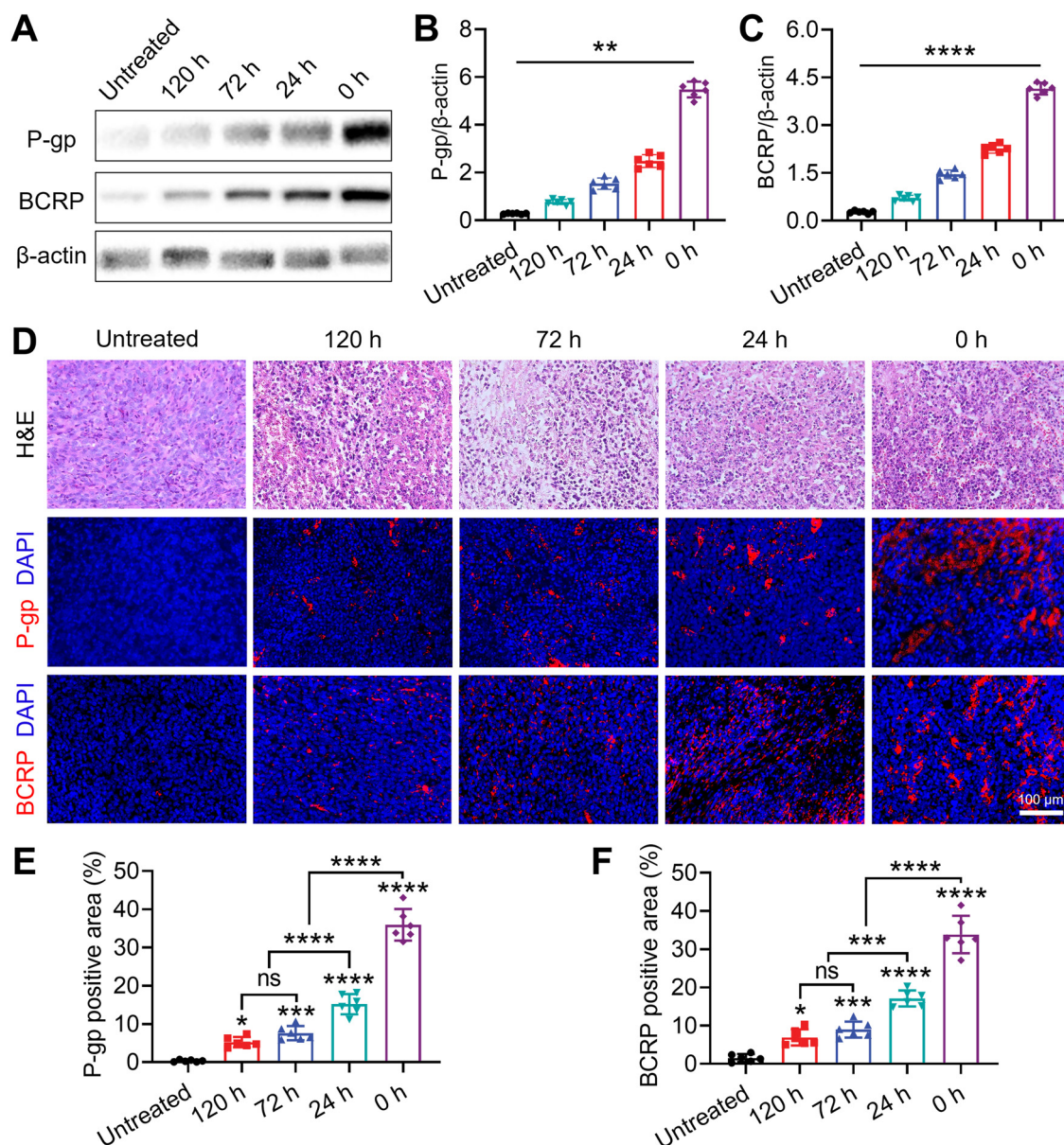
Fig. 7 – Multi-drug resistance-associated protein expression in TNBC tumors following dose density variation of local dose-dense AC therapy. (A) Representative P-gp and BCRP protein expression of 4T1-Luc2 tumors analyzed by western blot assay at 42 d after device implantation. (B-C) Relative expression levels of (B) P-gp and (C) BCRP proteins from western blot analysis. (D) Representative H&E and immunohistochemical (P-gp, BCRP) staining results of tumor sections at day 42 (Scale bar: 100 μm). (E and F) Quantitative analysis of (E) P-gp and (F) BCRP positive cells in the harvested TNBC tumors from data in (D). All data are shown as means ± SD ($n = 6$). *$P < 0.05$, **$P < 0.01$, ***$P < 0.001$, ****$P < 0.0001$.

pulses, and we applied this strategy to enhance the anti-cancer effect of local dose-dense AC chemotherapy. This strategy could be considered for chemotherapy based on local drug delivery systems and other studies that aim to increase treatment efficiency by reducing drug resistance.

4.   Conclusion

In summary, we developed local dose-dense AC chemotherapy using 3D printed devices, demonstrating remarkable efficacy in the metastatic TNBC model. We effectively suppressed tumor growth, metastasis, and drug resistance response by precisely controlling the dose density through time-programmed pulsatile release. Moreover, using 3D printed devices offers numerous clinical benefits, such as using biodegradable materials, minimally invasive implantation procedures, and superior anti-cancer effectiveness compared to IT administration. Considering the adverse effects of systemic administration approaches, we believe the developed platform can be a promising strategy to enhance therapeutic efficiency by transitioning from systemic

to local delivery for therapies with complex dosing schedules.

Conflicts of interest

The authors report no conflicts of interest. The authors alone are responsible for the content and writing of this article.

Acknowledgements

Supplementary materials

Supplementary material associated with this article can be found, in the online version, at doi:10.1016/j.ajps.2024.100884.

REFERENCES

[1] Giaquinto AN, Sung H, Miller KD, Kramer JL, Newman LA, Minihan A, et al. Breast cancer statistics, 2022. CA Cancer J Clin 2022;72:524–41.

[2] Zagami P, Carey LA. Triple negative breast cancer: pitfalls and progress. Npj Breast Cancer 2022;8:95.

[3] Almansour NM. Triple-negative breast cancer: a brief review about epidemiology, risk factors, signaling pathways, treatment and role of artificial intelligence. Front Mol Biosci 2022;9:836417.

[4] Bianchini G, Balko JM, Mayer IA, Sanders ME, Gianni L. Triple-negative breast cancer: challenges and opportunities of a heterogeneous disease. Nat Rev Clin Oncol 2016;13:674–90.

[5] Siddiqui M, Rajkumar SV. The high cost of cancer drugs and what we can do about it. Mayo Clin Proc 2012;87:935–43.

[6] Cha Y, Erez T, Reynolds IJ, Kumar D, Ross J, Koytiger G, et al. Drug repurposing from the perspective of pharmaceutical companies. Br J Pharmacol 2018;175:168–80.

[7] Gonzalez-Angulo AM, Stemke-Hale K, Palla SL, Carey M, Agarwal R, Meric-Berstam F, et al. Androgen receptor levels and association with PIK3CA mutations and prognosis in breast cancer. Clin Cancer Res 2009;15:2472–8.

[8] Wang W, Oguz G, Lee PL, Bao Y, Wang P, Terp MG, et al. KDM4B-regulated unfolded protein response as a therapeutic vulnerability in PTEN-deficient breast cancer. J Exp Med 2018;215:2833–49.

[9] Paridaens R, Van Aelst F, Georgoulias V, Samonnig H, Cocquyt V, Zielinski C, et al. A randomized phase II study of alternating and sequential regimens of docetaxel and doxorubicin as first-line chemotherapy for metastatic breast cancer. Ann Oncol 2003;14:433–40.

[10] Ocaña A, Hortobagyi GN, Esteva FJ. Concomitant *versus* sequential chemotherapy in the treatment of early-stage and metastatic breast cancer. Clin Breast Cancer 2006;6: 495–504.

[11] Gray R, Bradley R, Braybrooke J, Liu Z, Peto R, Davies L, et al. Increasing the dose intensity of chemotherapy by more frequent administration or sequential scheduling: a patient-level meta-analysis of 37 298 women with early breast cancer in 26 randomised trials. Lancet 2019;393:1440–52.

[12] Zhang L, Yu Q, Wu XC, Hsieh MC, Loch MM, Chen VW, et al. Impact of chemotherapy relative dose intensity on cause-specific and overall survival for stage I–III breast cancer: ER+/PR+, HER2- *vs.* triple-negative. Breast Cancer Res Treat 2018;169:175–87.

[13] Amir E, Ocana A, Freedman O, Clemons M, Seruga B. Dose-dense treatment for triple-negative breast cancer. Nat Rev Clin Oncol 2010;7:79–80.

[14] Simon R, Norton L. The Norton–Simon hypothesis: Designing more effective and less toxic chemotherapeutic regimens. Nat Clin Pract Oncol 2006;3:406–7.

[15] Citron ML. Dose-dense chemotherapy: Principles, clinical results and future perspectives. Breast Care 2008;3:251–5.

[16] Morris PG, McArthur HL, Hudis C, Norton L. Dose-dense chemotherapy for breast cancer: what does the future hold? Futur Oncol 2010;6:951–65.

[17] Fornier M, Norton L. Dose-dense adjuvant chemotherapy for primary breast cancer. Breast Cancer Res 2005;7:64.

[18] Kr A. Dose dense neoadjuvant and adjuvant chemotherapy in triple-negative breast cancer patients: survival analysis. Ann Oncol 2019;30:iii37.

[19] Wolinsky JB, Colson YL, Grinstaff MW. Local drug delivery strategies for cancer treatment: Gels, nanoparticles, polymeric films, rods, and wafers. J Control Release 2012;159:14–26.

[20] Zhou Z, Liu Y, Jiang X, Zheng C, Luo W, Xiang X, et al. Metformin modified chitosan as a multi-functional adjuvant to enhance cisplatin-based tumor chemotherapy efficacy. Int J Biol Macromol 2023;224:797–809.

[21] Gao W, Liang Y, Peng X, Hu Y, Zhang L, Wu H, et al. *In situ* injection of phenylboronic acid based low molecular weight gels for efficient chemotherapy. Biomaterials 2016;105:1–11.

[22] Westphal M, Hilt DC, Bortey E, Delavault P, Olivares R, Warnke PC, et al. A phase 3 trial of local chemotherapy with biodegradable carmustine (BCNU) wafers (Gliadel wafers) in patients with primary malignant glioma. Neuro Oncol 2003;5:79–88.

[23] Chao Y, Liang C, Tao H, Du Y, Wu D, Dong Z, et al. Localized cocktail chemoimmunotherapy after *in situ* gelation to trigger robust systemic antitumor immune responses. Sci Adv 2020;6:eaaz4204.

[24] Zhao D, Hu C, Fu Q, Lv H. Combined chemotherapy for triple negative breast cancer treatment by paclitaxel and niclosamide nanocrystals loaded thermosensitive hydrogel. Eur J Pharm Sci 2021;167:105992.

[25] Jusu SM, Obayemi JD, Salifu AA, Nwazojie CC, Uzonwanne V, Odusanya OS, et al. Drug-encapsulated blend of PLGA-PEG microspheres: *In vitro* and *in vivo* study of the effects of localized/targeted drug delivery on the treatment of triple-negative breast cancer. Sci Rep 2020;10:14188.

[26] Lu X, Miao L, Gao W, Chen Z, McHugh KJ, Sun Y, et al. Engineered PLGA microparticles for long-term, pulsatile release of STING agonist for cancer immunotherapy. Sci Transl Med 2020;12:eaaz6606.

[27] Park CG, Hartl CA, Schmid D, Carmona EM, Kim HJ, Goldberg MS. Extended release of perioperative immunotherapy prevents tumor recurrence and eliminates metastases. Sci Transl Med 2018;10:eaar1916.

[28] Gao Y, Wang J, Han H, Xiao H, Jin W, Wang S, et al. A nanoparticle-containing polycaprolactone implant for combating post-resection breast cancer recurrence. Nanoscale 2021;13:14417–25.

[29] Li X, He Y, Hou J, Yang G, Zhou S. A Time-programmed release of dual drugs from an implantable trilayer structured fiber device for synergistic treatment of breast cancer. Small 2020;16:1902262.

[30] Li J, Li J, Yao Y, Yong T, Bie N, Wei Z, et al. Biodegradable electrospun nanofibrous platform integrating antiplatelet therapy-chemotherapy for preventing postoperative tumor recurrence and metastasis. Theranostics 2022;12:3503–17.

[31] Dang HP, Shafiee A, Lahr CA, Dargaville TR, Tran PA. Local doxorubicin delivery via 3D-printed porous scaffolds reduces systemic cytotoxicity and breast cancer recurrence in mice. Adv Ther 2020;3:2000056.

[32] Shi X, Cheng Y, Wang J, Chen H, Wang X, Li X, et al. 3D printed intelligent scaffold prevents recurrence and distal metastasis of breast cancer. Theranostics 2020;10:10652–64.

[33] Norton L. Evolving concepts in the systemic drug therapy of breast cancer. Semin Oncol 1997;24:S10.3–S10.10.

[34] Chin SY, Poh YC, Kohler AC, Compton JT, Hsu LL, Lau KM, et al. Additive manufacturing of hydrogel-based materials for next-generation implantable medical devices. Sci Robot 2017;2:eaah6451.

[35] Mirvakili SM, Langer R. Wireless on-demand drug delivery. Nat Electron 2021;4:464–77.

[36] Wei X, Liu C, Wang Z, Luo Y. 3D printed core-shell hydrogel fiber scaffolds with NIR-triggered drug release for localized therapy of breast cancer. Int J Pharm 2020;580:119219.

[37] Talebian S., Foroughi J., Wade S.J., Vine K.L., Dolatshahi-Pirouz A., Mehrali M., et al. Biopolymers for antitumor implantable drug delivery systems: recent advances and future outlook. Adv Mater n.d.;30:1706665.

[38] Kevadiya BD, Ottemann BM, Ben Thomas M, Mukadam I, Nigam S, McMillan J, et al. Neurotheranostics as personalized medicines. Adv Drug Deliv Rev 2019;148:252–89.

[39] Emi TT, Barnes T, Orton E, Reisch A, Tolouei AE, Madani SZM, et al. Pulsatile chemotherapeutic delivery profiles using magnetically responsive hydrogels. ACS Biomater Sci Eng 2018;4:2412–23.

[40] Myung N, Jin S, Cho HJ, Kang HW. User-designed device with programmable release profile for localized treatment. J Control Release 2022;352:685–99.

[41] Kwon SK, Song JJ, Cho CG, Park SW, Choi SJ, Oh SH, et al. Polycaprolactone spheres and theromosensitive pluronic F127 hydrogel for vocal fold augmentation: *in vivo* animal study for the treatment of unilateral vocal fold palsy. Laryngoscope 2013;123:1694–703.

[42] Yi HG, Choi YJ, Kang KS, Hong JM, Pati RG, Park MN, et al. A 3D-printed local drug delivery patch for pancreatic cancer growth suppression. J Control Release 2016;238:231–41.

[43] Singh R, Kumar B, Sahu RK, Kumari S, Jha CB, Singh N, et al. Development of a pH-sensitive functionalized metal organic framework: *In vitro* study for simultaneous delivery of doxorubicin and cyclophosphamide in breast cancer. RSC Adv 2021;11:33723–33.

[44] Park MK, Lee CH, Lee H. Mouse models of breast cancer in preclinical research. Lab Anim Res 2018;34:160–5.

[45] Choi SB, Park JM, Ahn JH, Go J, Kim J, Park HS, et al. Ki-67 and breast cancer prognosis: Does it matter if Ki-67 level is examined using preoperative biopsy or postoperative specimen? Breast Cancer Res Treat 2022;192:343–52.

[46] Kim GM, Kim JH, Kim JH, Cho YU, Kim SI, Park S, et al. A phase II study to evaluate the safety and efficacy of pegteograstim in Korean breast cancer patients receiving dose-dense doxorubicin/cyclophosphamide. Cancer Res Treat 2019;51:812–18.

[47] Nair A, Morsy MA, Jacob S. Dose translation between laboratory animals and human in preclinical and clinical phases of drug development. Drug Dev Res 2018;79:373–82.

[48] Kim HR, Cho YS, Chung SW, Choi JU, Ko YG, Park SJ, et al. Caspase-3 mediated switch therapy of self-triggered and long-acting prodrugs for metastatic TNBC. J Control Release 2022;346:136–47.

[49] Sanguineti G, Del Mastro L, Guenzi M, Ricci P, Cavallari M, Canavese G, et al. Impact of chemotherapy dose-density on radiotherapy dose-intensity after breast conserving surgery. Ann Oncol 2001;12:373–8.

[50] Nanda R, Liu MC, Yau C, Shatsky R, Pusztai L, Wallace A, et al. Effect of pembrolizumab plus neoadjuvant chemotherapy on pathologic complete response in women with early-stage breast cancer: An analysis of the ongoing phase 2 adaptively randomized I-SPY2 trial. JAMA Oncol 2020;6:676–84.

[51] Liu Y, Zhou Z, Hou J, Xiong W, Kim H, Chen J, et al. Tumor selective metabolic reprogramming as a prospective PD-L1 depression strategy to reactivate immunotherapy. Adv Mater 2022;34:2206121.

[52] Wang H, Najibi AJ, Sobral MC, Seo BR, Lee JY, Wu D, et al. Biomaterial-based scaffold for *in situ* chemo-immunotherapy to treat poorly immunogenic tumors. Nat Commun 2020;11:5696.

[53] Cancer multidrug resistance. Nat Biotechnol 2000;18(Suppl 10):IT18–20.

[54] Dufour R, Daumar P, Mounetou E, Aubel C, Kwiatkowski F, Abrial C, et al. BCRP and P-gp relay overexpression in triple negative basal-like breast cancer cell line: a prospective role in resistance to Olaparib. Sci Rep 2015;5:12670.